Ore Geology Reviews 78 (2016) 58–68

Contents lists available at ScienceDirect

Ore Geology Reviews

journal homepage: www.elsevier.com/locate/oregeorev

Zinc and lead isotope signatures of the Zhaxikang Pb−−Zn deposit, South Tibet: Implications for the source of the ore-forming metals

Jilin Duan [a,b,*], Juxing Tang [a], Bin Lin [b,**]

[a] State Key Laboratory of Geological Processes and Mineral Resources, China University of Geosciences, Beijing 100083, China
[b] MLR Key Laboratory of Metallogeny and Mineral Resource Assessment, Institute of Mineral Resources, Chinese Academy of Geological Sciences, Beijing 100037, China

ARTICLE INFO

Article history:
Received 13 January 2016
Received in revised form 22 March 2016
Accepted 28 March 2016
Available online 2 April 2016

Keywords:
Zinc isotopes
Lead isotopes
Ore deposit
Zhaxikang
Tibet

ABSTRACT

Stable Zn isotopes may be applied to trace the source of ore-forming metals in various types of Pb—Zn deposits. To test this application, Zn and Pb isotope systematics for sulfides and associated basement rocks as well as Fe—Mn carbonates (gangue) from the Zhaxikang Pb—Zn deposit in South Tibet have been analyzed. The basement in this region includes metamorphosed mafic to felsic rocks (dolerite, quartz diorite, rhyolite porphyry, pyroclastics and porphyritic monzogranite). These rocks have similar δ^{66}Zn values of 0.33 to 0.37‰, with an average value of 0.36 ± 0.03‰ (2σ), except for the more evolved porphyritic monzogranite that has a heavier value of 0.49‰. Fe—Mn carbonates are present as hydrothermal veins and were probably precipitated from magmatic fluids. They have an average δ^{66}Zn value of 0.27 ± 0.05‰, which is slightly lighter than the basement rocks, possibly representing δ^{66}Zn isotopic compositions of the hydrothermal fluids. Sphalerite and galena have similar Zn isotopic compositions with δ^{66}Zn ranging from 0.03 to 0.26‰ and 0.21 to 0.28‰, respectively. Considering the Zn isotope fractionation factor between sphalerite and fluids of −0.2‰ at ~300 °C as reported in literature, hydrothermal fluids from which these sulfides precipitated will have δ^{66}Zn values of ca. 0.39 ± 0.10‰, which are consistent with the values of basement rocks and the Fe—Mn carbonates. This similarity supports a magmatic-hydrothermal origin of the Zhaxikang Pb—Zn deposit. Both Pb and S isotopes in these sphalerite and galena show large variations and are consistent with being derived from a mixture of basement and sedimentary rocks in various proportions. Zn isotopic compositions of the sulfides significantly extend the range of regional basement rocks, suggesting that sedimentary rocks (e.g., shales) are also a significant source of Zn. However, the Zn isotopic compositions of sphalerite and galena differ from those of marine carbonates and those of typical SEDEX-type deposits (e.g. Kelley et al., 2009), confirming a magmatic-hydrothermal model. Combined with regional geological observations and the age constraints of ~20 Ma (Zheng et al., 2012, 2014), the results of our investigation indicate that the Zhaxikang Pb—Zn deposit is most likely a magmatic-hydrothermal deposit.

1. Introduction

Zinc has five stable isotopes, which are: ^{64}Zn (48.63%), ^{66}Zn (27.90%), ^{67}Zn (4.10%), ^{68}Zn (18.75%) and ^{70}Zn (0.62%) (Rosman, 1972). With the development of the multi-collector inductively-coupled plasma mass spectrometer (MC-ICP-MS), precise and accurate Zn isotopic measurements are now possible. Maréchal et al. (1999) were the first to publish the measurement of Cu and Zn isotopic ratios in a variety of minerals and biological materials. Maréchal et al. (2000) and Pichat et al. (2003) demonstrated significant Zn isotope variations in ferromanganese nodules, sediment trap material, and marine carbonate. Maréchal et al. (1999) and Zhu et al. (2002) confirmed the broad range of Zn isotopic variations in copper ore observed by the earlier workers. To date, natural variations of >3‰ have been reported for Zn isotopes (expressed as δ^{66}Zn relative to JMC-Lyon).

In recent years, Zn isotopes are becoming increasingly applied and may be used as a tool for understanding the geochemical processes of zinc transportation and deposition in hydrothermal systems (e.g. Gagnevin et al., 2012; John et al., 2008; Kelley et al., 2009; Mason et al., 2005; Toutain et al., 2008; Zhou et al., 2014a, 2014b). Thus, zinc isotopes may be used to trace fluid pathways and sulfide precipitation. For example, the evolution of fluids from early to late stages, residual fluids and late-stage precipitates should have heavy Zn isotopic composition due to lighter Zn isotopic composition of sulfides than fluids from which the sulfides precipitated (John et al., 2008; Kelley et al., 2009; Mason et al., 2005; Sivry et al., 2008; Wilkinson et al., 2005; Dekov et al., 2010).

Pb—Zn deposits represent the most important resource of Zn worldwide. The four most common Pb—Zn mineral systems worldwide

* Correspondence to: J. Duan, State Key Laboratory of Geological Processes and Mineral Resources, China University of Geosciences, Beijing 100083, China.
** Correspondence to: B. Lin, Metallogeny and Mineral Resource Assessment, Institute of Mineral Resources, Chinese Academy of Geological Sciences, Beijing 100037, China.
E-mail addresses: duanjlynn@hotmail.com (J. Duan), linmengqiao@foxmail.com (B. Lin).

http://dx.doi.org/10.1016/j.oregeorev.2016.03.019
0169-1368/

include: (1) sedimentary exhalative (SEDEX) formed in continental margin or rift settings and hosted by carbonate or carbonaceous shale, (2) Mississippi Valley (MVT) associated with sedimentary rocks (mainly carbonate), (3) volcanic-hosted massive sulfides (VHMS); and (4) magmatic-hydrothermal related to igneous activity (Maréchal et al., 1999). To date, sulfur and lead isotopes have been commonly used to trace the source of metals and to constrain the origin of Pb—Zn deposits. In fact, there are also significant differences in Zn isotopic compositions among various crustal sources. The silicate Earth has an average δ^{66}Zn value of 0.28 ± 0.05‰ (Chen et al., 2013), deep seawaters have an average δ^{66}Zn of ~0.50‰ (Little et al., 2014; Zhao et al., 2014), whereas marine carbonate is isotopically heavy (up to ~1.3‰; Pichat et al., 2003; Kunzmann et al., 2013). These differences suggest that Zn isotopes may be used to distinguish different sources of zinc. However, few studies have attempted to investigate the application of Zn isotopes as a tracer of metal source through studying the deposits with well-characterized S and Pb isotope signatures (Gagnevin et al., 2012; Zhou et al., 2014a, 2014b).

In this paper, we report a case study on Zn and Pb isotopes in sphalerite, galena, basement rocks, and Fe—Mn carbonates veins from the Zhaxikang Pb—Zn deposit. Zhaxikang is in South Tibet and is one of the largest Pb—Zn deposits in China with a resource of 1.23 Mt Pb—Zn—Sb—Ag (with an average 3.36% for Pb—Zn—Sb), and 1803 t Ag (with an average of 88.75 g/t). The origin of this deposit is debated. Proposed models include SEDEX-type reworked by hydrothermal fluids based on C—O isotope studies (Zheng et al., 2012), low-sulfidation epithermal hot-spring type, based on silicate isotope systematics (Meng et al., 2008), or magmatic based on multi-isotopes and fluid inclusion studies (Lin, 2014; Zhu et al., 2012; Li, 2010). Our results indicate that formation of Zhaxikang is probably related to magmatic-hydrothermal activity.

2. Geological settings and samples

2.1. Tectonic background and regional geology

The Indus-Yarlung Zangbo (IYS) and Bangong-Nujiang (BNS) sutures divide the Tibetan Plateau into the Tethyan Himalaya orogen in the south, Lhasa Terrane in the centre, and Qiangtang Terrane in the north (Fig. 1A). The Tethyan Himalayan Orogen includes four eastward trending terranes named the Songpan–Ganze Terrane in the north through the Qiangtang and Lhasa terranes to the Himalaya Terrane in the south (Kapp et al., 2007).

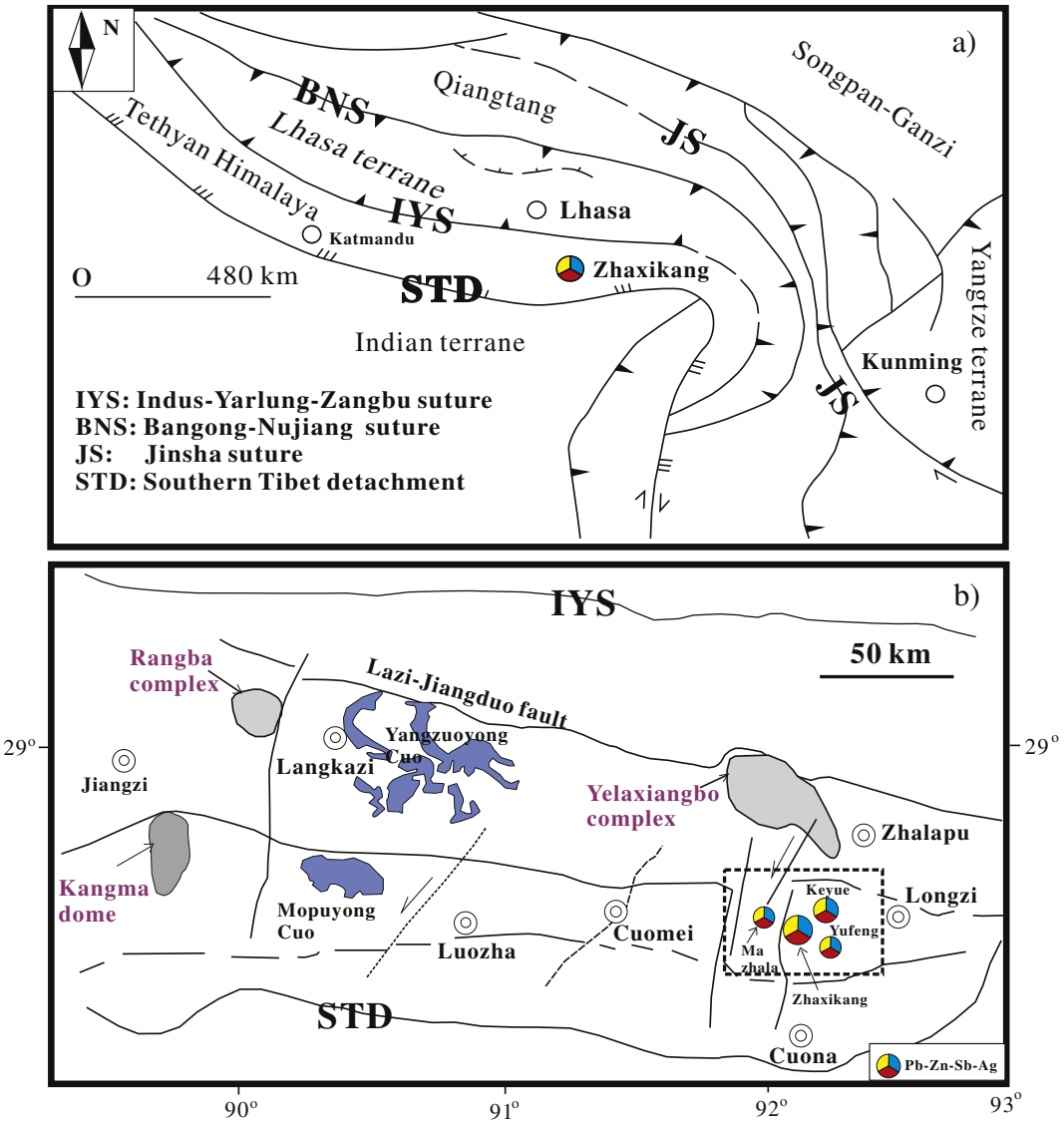

Fig. 1. Location of the study area in Tibetan Plateau (A). Distribution of similar-aged Pb—Zn deposits around the study area in Southern Tibet (B) (after Yin, 2001).

Zhaxikang is located in the southeastern part of the Tethys-Himalaya orogen (Fig. 1A; Yin et al., 1999; Yin, 2001). Detailed regional settings for the deposit have been reported in many previous studies (e.g. Yang et al., 2006, 2009; Zhang et al., 2010; Zhu et al., 2012; Zheng et al., 2012; Wang et al., 2012). The rocks in the region comprise the Precambrian Kangma-Longzi Formation and Mesozoic meta-sedimentary rocks. Regional deformations are related to collision and extension between the India and Eurasia plates, from 65 Ma to the present. Large-scale east-trending and north-dipping thrusts and folds, which related to the South Tibetan detachment system (STD) in the Tethyan Himalayan Orogen, were formed at about 23 Ma. They are crossed by north-trending and west-dipping transtensional normal faults which developed at ca. 18 Ma. Previous studies suggest that the multi-phases activities along eastward trending faults represent the main structure for regional basement rocks. These activities control the conduits for the flow of magma-hydrothermal fluids. On the other hand, northward-

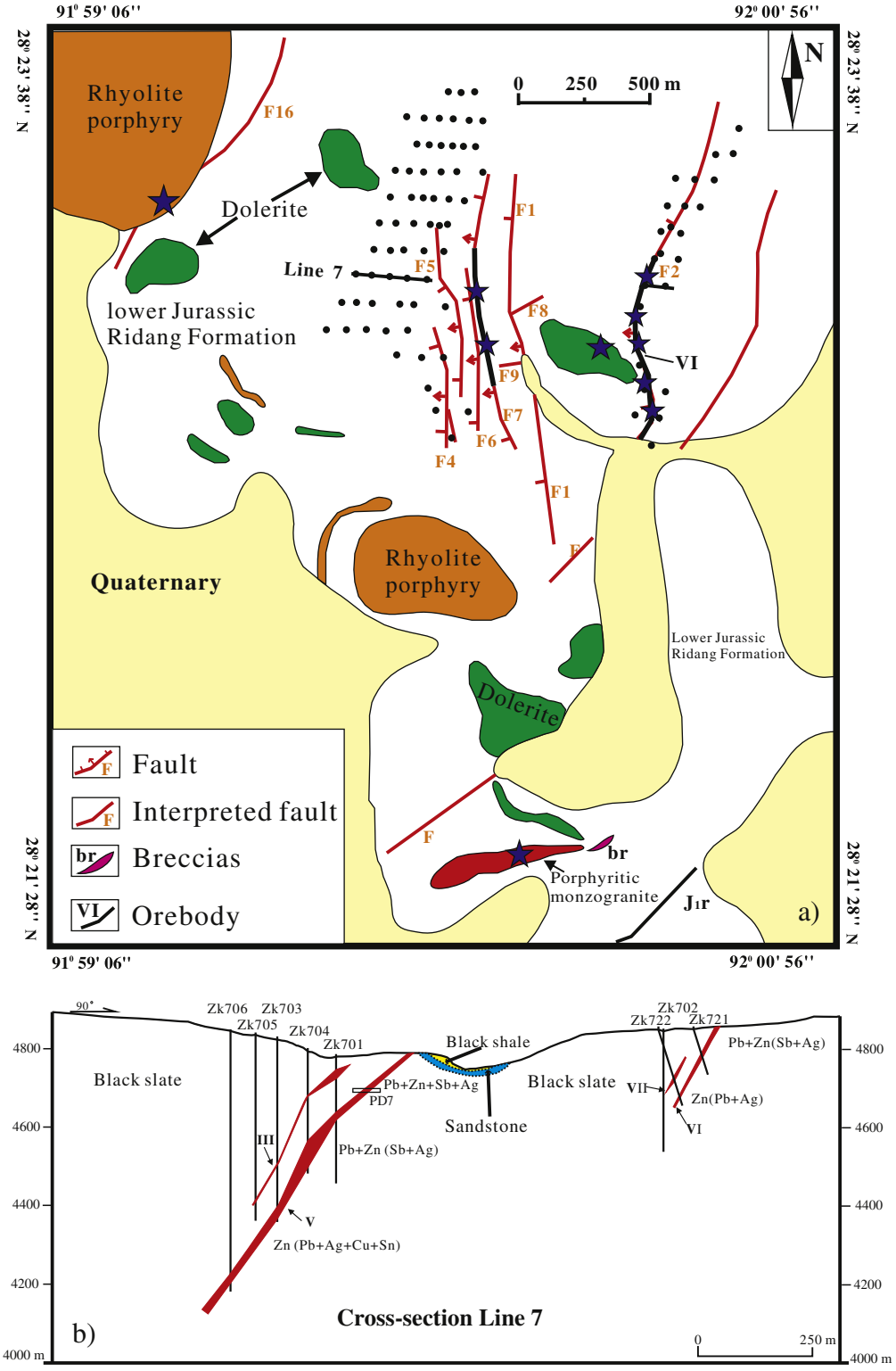

Fig. 2. Regional geological map of the Zhaxikang deposit (A). Stars represent the sampling localities. Cross-section for Line 7 in the Zhaxikang Pb—Zn deposit (B).

trending faults provided the pathway and space for regional metallogenic processes (Nie et al., 2005; Yang et al., 2006). Regional folding was well developed due to thrusts and nappes during the collision process, with the development of metamorphic core complex such as Yelaxiangbo complex (Fig. 1B), which is mainly composed of breccias and metamorphic rocks. These complexes have high-strain structures, controlled by eastward-trending faults. The peripheral area of these core complexes are composed of strongly deformed tectonic metamorphic rocks and Cenozoic leucogranites.

2.2. Deposit geology

The rocks at the Zhaxikang Pb—Zn deposit consist of the Triassic Nieru Formation overlain by and faulted against the Jurassic Ridang Formation. The Ridang Formation is also partly covered by Quaternary sediments (Fig. 2).

The Ridang Formation consists of neritic-facies sedimentary rocks, which were deposited in a tidal environment (Liang et al., 2013; Lin et al., 2013; Lin, 2014). The formation includes a lower part, white-brown quartz sandstone and shale located in the southwestern part of the Zhaxikang mine, covered by grey-black shale in the eastern and northern parts of the mine; an upper part, fine- to medium-grained, grey-green quartz sandstone in the central part of the mine area, a grey-black carbonaceous shale interbedded with brown-yellow calcareous sandstone in the central and partial areas of the mineralization, and an upper succession of grey-green quartz sandstone interbedded with grey-black shale and thin-bedded limestone.

The Zhaxikang Pb—Zn deposit has a resource of 1.23 Mt Pb—Zn—Sb (with a combined grade of 3.36% for Pb—Zn—Sb), and 8300 t Ag ore (@ 88.75 g/t Ag). The deposit is located in the southeastern part of the Yangzhuoyongcuo–Nariyongcuo Syncline which located in the northern Tethyan Himalayan orogen (Fig. 2). The age of the Zhaxikang Pb—Zn deposit is still debated. Zheng et al. (2014) and Lin (2014) document Rb—Sr dates from pyrite and sphalerite and U—Pb from hydrothermal zircons that range from 147 to 14 Ma. Several Pb—Zn deposits with similar ages are located around Zhaxikang, including Yufeng, Mazhala, and Keyue (Fig. 2; Yin et al., 1999; Zheng et al., 2014).

Intense tectonic activity and related deformation events, are associated with ore formation, and are recognised in the Zhaxikang mine area. The main faults are F7 and F2, which control the V and VI orebodies respectively (Fig. 2). F7 is located in the west, strikes north to south and dips west and was preceded by several periods of deformations. There are several generations of tectonic breccias in this fault zone, with accompanying alteration and Pb—Zn mineralization. The F2 fault is in the western mining area, which is north-striking and west-dipping. It hosts the VI orebody with abundant tectonic breccias, mineralization and alteration.

Igneous rocks are well developed in the region. Both mafic and felsic rocks are exposed, and include the Cambrian porphyritic monzogranite, early Cretaceous dolerite, rhyolite porphyry, and Miocene leucogranites (Fig. 2). These igneous rocks have a wide age range from ~21 to 135 Ma (Lin, 2014). Rhyolite porphyry mainly occurs in the west and south of the deposit and is gray with a pale yellow weathered surface. Rhyolite porphyry displays such vesicular texture and is mainly composed of quartz phenocrysts and plagioclase (with ~5% feldspar, biotite and muscovite). It has strong alterations including carbonate, silicification, sericite and chlorite. Dolerite occurs as EW-trending dykes, gray-green in colour with a fine-grained texture. The mineral assemblages mainly consist of plagioclase and pyroxene with scarce hornblende, quartz, ilmenite, and pyrite. The porphyritic monzogranite is partially exposed to the southwest of the deposit. Its phenocrysts include quartz, plagioclase, muscovite, and biotite, which are surrounded by felsic matrix. The plagioclase is variably altered to silica (quartz), carbonate and sericite. The leucogranite is a two-mica granite or monzonite mica granite with porphyritic and granular textures, massive and gneissic structure. Its phenocrysts are muscovite, biotite, quartz, plagioclase with minor tourmaline (<5%). The presence of linear fabrics hint some deformation, leading to a gneissic structure.

2.3. Mineralogy and samples

Ore minerals in the studied samples include galena, sphalerite, pyrite, stibnite, arsenopyrite, boulangerite, jamesonite and chalcopyrite, with minor freibergite, pyrrhotite, andorite, bournonite and few supergene minerals such as limonite and malachite (Table 1; Fig. 3). There are also quartz, iron-manganese carbonate, chlorite and sericite. Hydrothermal breccias are present in this area. They occur as vein or vein-like, banded, fractured structures (Wang et al., 2012).

The alteration of the host rocks is relatively weak and occurs mainly in the mineralized fracture zone. The main alteration in the wall rock consists of: iron-manganese carbonate, silicification, carbonates, sericite, chlorite and late supergene alteration (Zhang, 2012). Iron-manganese carbonate (Fe—Mn carbonates) is related to early-stage lead-zinc mineralization, formed by hydrothermal infilling probably related to deformation events (Fig. 3g, h and i). The fluid inclusions in Fe—Mn carbonates yield homogenization temperatures ranging from 190 to 288 °C, with a median (value of a quantity at the midpoint of a frequency distribution) temperature of 242 °C (Lin, 2014). The salinity ranges from 1.40 to 10.11 wt% NaCl eqv (average = 4.85 wt% NaCl eqv) (Lin, 2014). The temperatures of early-stage Pb—Zn hydrothermal mineralization is from190 to 288 °C, with a median temperature of 251 °C. Its salinity ranges from 4.03 to 10.11 wt% NaCl eqv (average = 5.3 wt% NaCl eqv). The late-stage Sb—Pb mineralization has an uniform temperature of 198 to 284 °C (median = 232 °C). The salinity ranges from 1.40 to 7.59 wt% NaCl eqv (average = 4.22 wt% NaCl). Overall, from early to late stages of mineralization, the homogenization temperature appears to decrease gradually (Zhu et al., 2012; Lin, 2014). >30 samples including regional basement rocks, sulfides and Fe—Mn carbonates have been used for this study.

3. Analytical methods

3.1. Lead isotope analysis

Lead isotopic ratios of sulfide separates (galena and sphalerite) were analyzed utilizing a New Wave 193 nm ArF excimer laser coupled with a Thermo Scientific Neptune MC-ICPMS at the Northwest University, China. This method has been previously outlined by Chen et al. (2014a) in detail. Samples were cut using a diamond blade saw, and sulfide-bearing pieces were then mounted in epoxy resin. The mounts were polished with oil-based diamond suspensions in grit size and then peeled off of the glass slide as well as polished to a flat surface. The sulfide samples were examined and imaged in reflected light, prior to isotope ratio analysis. The sample surface was carefully cleaned by anhydrous ethanol to erase any potential contamination prior to laser ablation analysis. The external accuracy of analysis of both $^{208}Pb/^{204}Pb$ and $^{207}Pb/^{204}Pb$ ratios was better than ±0.1% based on routine measurements of standards (Chen et al., 2014a).

3.2. Zinc isotope analysis

Silicate rock samples were weighed to contain at least 0.4 mg Zn for isotopic analysis (Liu et al., 2014; Lv et al., 2016). The Zn contents of these silicate rock samples are measured by ICPMS before the test of Zn isotope. The samples were dissolved in a 1:1 (v/v) mixture of double-distilled HF and HNO_3 in Savillex screw-top beakers, followed by heating at 160 °C on a hotplate in an exhaust hood (Class 100). The solutions were dried down at 150 °C to expel the fluorine. The dried residues were refluxed with a 1:3 (v/v) mixed HNO_3 and HCl, followed by heating and then evaporating to dryness at 80 °C. The samples were refluxed with concentrated HNO_3 until complete dissolution was achieved, and subsequently dried down at 80 °C. Sulfide separates

Table 1
Mineral paragenesis of the Zhaxikang Pb—Zn deposit.

Periods	Hydrothermal							Supergene
Stages	Stage I				Stage II			
Mineral assemblages	Cal + Sp	Gn + Sp + Py + Apy	Sp + Cal + Gn	Qz + sulfate	Qz + Cpy	Py + Cpy	Qz	
Calcite	—							
Quartz	—	—	—	—	—	—	—	
Sericite	—						—	
Chlorite	—							
Fe-Mn carbonates	—	—	—					
Sphalerite	—	—	—	—				
Galena	—	—	—					
Stibnite				—	—			
Boulangerite				—				
Freibergite		—	—	—				
Chalcopyrite	—	—	—			—		
Pyrite	—	—	—	—		—		
Arsenopyrite	—	—	—	—				
Bournonite		—	—					—
Szaskaite								—
Limonite								—
Malachite								—

Cal, calcite; Py, pyrite; Sp, sphalerite; Gn, galena; Qz, quartz; Apy, arsenopyrite.
— Less; — More.

were hand-picked under a binocular microscope. After complete dissolution of the samples, for both silicate rocks and sulfides, 1 ml of 8 N HCl + 0.001% H_2O_2 was added to the beaker and heated to dryness at 80 °C. This process was repeated and the final material was dissolved in 1 ml of 8 N HCl in preparation for ion-exchange separation. Zinc was purified by a single column ion-exchange chromatography using Bio-Rad strong anion resin AG-MP-1 M (Liu et al., 2014; Lv et al., 2016). Copper was eluted in 24 ml 8 N HCl, followed by Fe and then Zn was collected in 10 ml 0.5 N HNO3 after the elution of Fe fraction. The Zn recovery is close to 100%, and the total procedural blank is 2 ng which is <0.1% of Zn (>2 μg) in the purified samples. Column chemistry is only not necessary for sphalerites and thus most of them were directly analyzed for Zn isotopic ratios after complete dissolution.

Zinc isotopic ratios were measured using the *Neptune plus* MC-ICP-MS at the Isotope Geochemistry Laboratory of the China University of Geosciences, Beijing. The sample-standard bracketing method was used in order to correct for instrumental mass fractionation (Borrok et al., 2007; Dauphas et al., 2009; Schoenberg and von Blanckenburg, 2005; Zhu et al., 2002). The in-house Zn standard solutions (GSB Zn) were used for bracketing the samples measured. Zn isotopic data are reported in standard δ-notation in per mil relative to the standard reference material JMC 3-0749L:

$$\delta^{66}Zn = \left(\left(^{66}Zn/^{64}Zn\right)_{sample}/\left(^{66}Zn/^{64}Zn\right)_{JMC} - 1\right)\cdot 1000.$$

The long-term external reproducibility for $\delta^{66}Zn$ measurements is better than ±0.05‰ based on repeated analysis of silicate rocks (2SD) (Lv et al., 2016). A series of international geostandards (BHVO-2, BCR-2 and BIR-1a) were analyzed during the course of this study. The measured $\delta^{66}Zn$ values of BHVO-2, BCR-2 and BIR-1a are 0.31 ± 0.05‰, 0.28 ± 0.04‰ and 0.29 ± 0.04‰, respectively. These values agree with those reported previously (Archer and Vance, 2004; Chen et al., 2013; Sossi et al., 2015) and confirm that the data obtained in this study are precise and accurate.

4. Results

4.1. Zn isotope data of sulfides

Zinc isotope data of sulfides (sphalerite and galena), regional igneous rocks and Fe—Mn carbonates from the Zhaxikang Pb—Zn polymetallic deposit are reported in Table 2 and plotted in Fig. 4. All samples, taken together, yield a slope of 1.83 ± 0. 17 ($R^2 = 0.95$) in the $\delta^{68}Zn$ versus $\delta^{66}Zn$ diagram (not shown), which is consistent within error with the theoretical value (2), indicating mass-dependent Zn isotope fractionation. The sphalerites from the Zhaxikang deposit have $\delta^{66}Zn$ values ranging from 0.03 to 0.25‰ with an average value of 0.18 ± 0.12‰ ($n = 20$; 2SD). $\delta^{66}Zn$ values of the galena display a smaller range from 0.19 to 0.28‰ with an average of 0.23 ± 0.08‰ ($n = 4$; 2SD).

4.2. Zn isotope data of silicate rocks and Fe—Mn carbonates

Igneous rocks from Zhaxikang range in composition from mafic to felsic (dolerite, quartz diorite, rhyolite porphyry and pyroclastics) and have a narrow range of $\delta^{66}Zn$ values varying from 0.33 to 0.37‰, with a mean of 0.36 ± 0.03‰ (2SD). The more evolved porphyritic monzogranite has a slightly heavier $\delta^{66}Zn$ value of 0.49 ± 0.03‰. The values of these basement rocks are generally similar to the values of mafic and felsic rocks reported to date (0.22–0.44‰; Zhu et al., 2002; Archer and Vance, 2004; Borrok et al., 2007; Chen et al., 2013). The Fe—Mn carbonates occur as veins cross-cutting the orebody and were precipitated from hydrothermal fluids (Lin, 2014). Two Fe—Mn carbonates have the same $\delta^{66}Zn$ value of 0.27‰ (Table 2).

4.3. Pb isotope data of sulfides

The Pb isotope data of sphalerite and galena from the Zhaxikang Pb—Zn deposit are reported in Table 3 and plotted in Fig. 5. A total of 21 spots have been analyzed. The $^{206}Pb/^{204}Pb$ ratios of sphalerites vary from 18.727 to 19.362, $^{207}Pb/^{204}Pb$ from 15.355 to 15.702, and $^{208}Pb/^{204}Pb$ from 38.685 to 39.826. The $^{206}Pb/^{204}Pb$ ratios of galenas vary from 19.686 to 19.896, $^{207}Pb/^{204}Pb$ from 15.851 to 15.900, and $^{208}Pb/^{204}Pb$ from 40.339 to 40.537. It is noted that galenas have significantly higher (more radiogenic) Pb isotopic ratios than sphalerites in the studied samples.

5. Discussion

In the following sections, we first discuss the Zn isotopic compositions of the regional basement rocks related to the mineralization. Then, combined with S and Pb isotope data, we discuss the processes

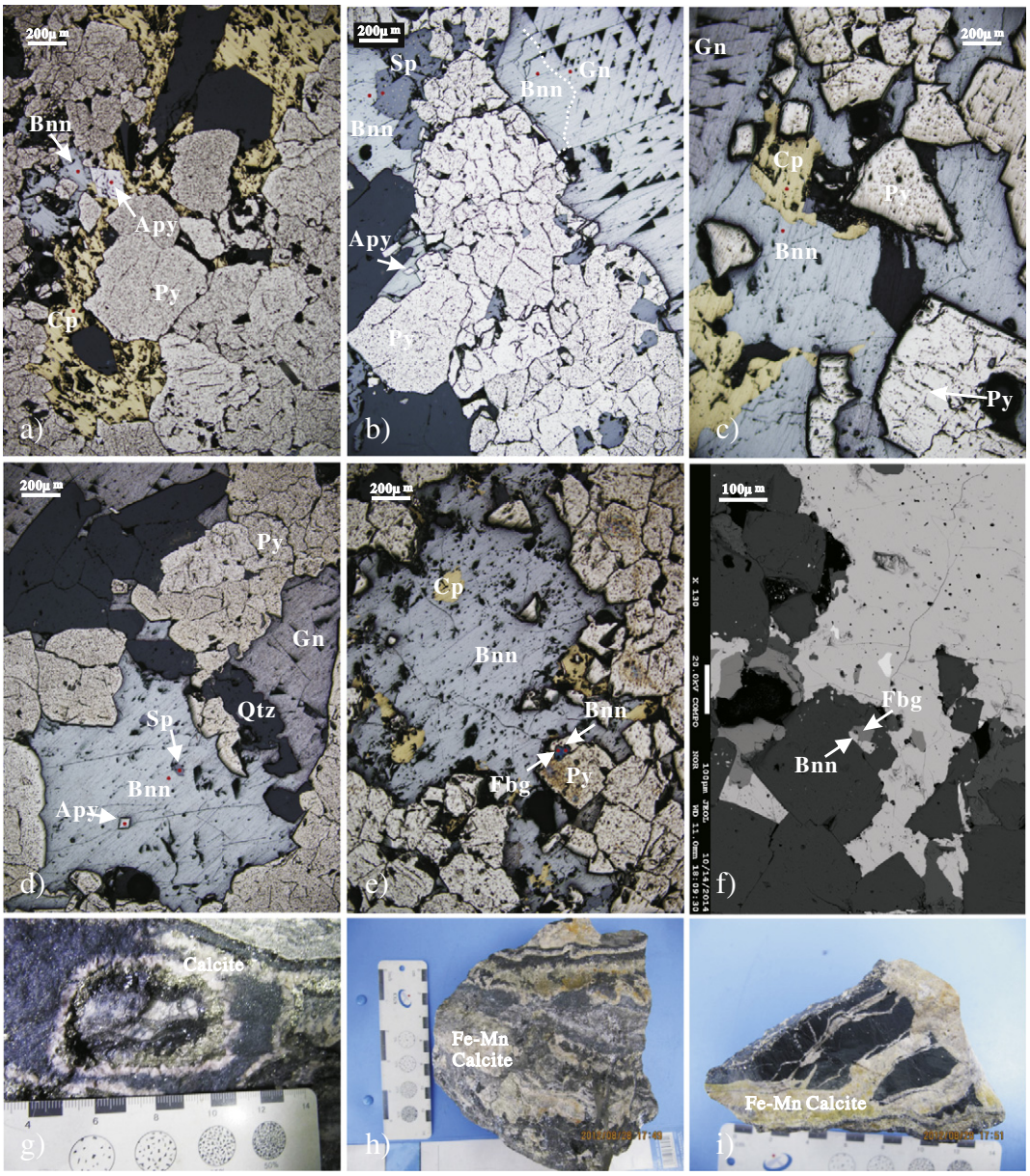

Fig. 3. Photomicrographs of ore minerals in the Zhaxikang Pb—Zn deposit. Sp: sphalerite; Gn: Galena; Py: pyrite; Cp: chalcopyrite; Fbg: Freibergite; Apy: Arsenopyrite; Bnn: Bournonite; Qtz: Quartz.

potentially fractionating Zn isotopes during ore-forming activity and the potential of using Zn isotopes to trace the source of ore metals. Finally, we discuss the origin of the Zhaxikang Pb—Zn deposit based on the new Zn and Pb isotope data.

5.1. Zn isotopic compositions of basement rocks in Zhaxikang

Previous studies show that basalts (MORBs and OIBs) commonly have quite similar δ^{66}Zn values of +0.28 ± 0.05‰ (Chen et al., 2013), whereas felsic igneous rocks have a significant range of δ^{66}Zn values (~0.12‰ to 0.88‰) (Telus et al., 2012; Chen et al., 2013; Sossi et al., 2015). In this study, most of the regional igneous rocks (mafic to felsic) spatially and temporally associated the Zhaxikang Pb—Zn deposit have a limited range of δ^{66}Zn values from +0.33 to +0.37‰ (mean = +0.36 ± 0.03‰) (Fig. 4), except the porphyritic monzogranite, which has a slightly heavier δ^{66}Zn value of 0.49‰ ± 0.05‰. Overall, these values fall within the range reported for mafic to felsic rocks in previous studies (e.g., Chen et al., 2013; Sossi et al., 2015). The studied porphyritic monzogranite also has a relatively lower Zn concentration, higher SiO_2 and lower MgO contents (Fig. 4). This may be consistent with a small Zn isotope fractionation during magmatic differentiation (Chen et al., 2013), although fluid exsolution is an alternative explanation for the heavy Zn isotopic composition of the most felsic granite (see Sossi et al., 2015) or at least it is a probability.

Compared with igneous rocks, other crustal reservoirs (marine carbonates, shales, river and seawater) have significantly different Zn isotopic compositions. For example, sedimentary marine carbonates have δ^{66}Zn ranging from 0.24 to 1.32‰ (Pichat et al., 2003), sedimentary rocks have δ^{66}Zn ranging from ca. −0.05 to 1.0‰ (Maréchal et al., 2000; Weiss et al., 2007; Bentahila et al., 2008; Lv et al., 2016; Little et al., 2016), and the deep seawater has an average δ^{66}Zn of 0.51‰ (Little et al., 2014; Zhao et al., 2014; John and Conway, 2014). Therefore, the variation of Zn isotopes in mineral systems can occur if there are multiple Zn sources with different Zn isotopic compositions. Especially, marine carbonates have very heavy δ^{66}Zn of up to +1.32‰ (average = 0.91‰) relative to igneous rocks (Pichat et al., 2003). Therefore, Zn isotope systematic may be an effective tool in distinguishing igneous rocks and carbonate sources.

Table 2
Zinc isotope data of silicate rocks and sulfides from the Zhaxikang Pb—Zn deposit, South Tibet.

Sample no.	Mineral	$\delta^{66}Zn$	2SD	$\delta^{68}Zn$	2SD	N	$\delta^{68}Zn/\delta^{66}Zn$	Comments
B1	Sp	0.18	0.03	0.37	0.06	3	1.99	No column
B1	Repeated	1.20	0.06	2.36	0.08	3	1.97	With column
B2	Sp	0.12	0.03	0.24	0.02	3	1.98	No column
B3	Sp	0.23	0.03	0.47	0.12	3	1.99	No column
B4	Sp	0.11	0.04	0.23	0.04	3	2.01	No column
B5	Sp	0.19	0.02	0.37	0.04	3	1.98	No column
B6	Sp	0.03	0.03	0.06	0.01	3	1.97	No column
B7	Sp	0.12	0.03	0.25	0.24	4	2.01	No column
B8	Sp	0.18	0.09	0.57	5.71	4	3.23	No column
B9	Sp	0.24	0.02	0.48	0.04	4	1.98	No column
B10	Sp	0.25	0.05	0.50	0.09	4	2.00	No column
B11	Sp	0.15	0.08	0.29	0.12	4	1.96	No column
B12	Sp	0.18	0.09	0.37	0.11	4	2.00	No column
B13	Sp	0.26	0.05	0.50	0.06	4	1.93	No column
B14	Sp	0.12	0.03	0.23	0.05	4	1.96	No column
B14	Repeated	1.12	0.03	2.18	0.05	4	1.96	With column
B15	Sp	0.15	0.06	0.30	0.04	3	1.99	No column
B16	Sp	0.22	0.03	0.44	0.05	3	1.99	No column
B17	Sp	0.23	0.05	0.45	0.02	3	1.95	No column
B18	Sp	0.22	0.02	0.44	0.08	3	1.96	No column
B19	Sp	0.24	0.03	0.48	0.01	3	1.98	No column
B21	Sp	0.18	0.03	0.35	0.01	3	2.00	No column
B3	Sd	0.27	0.05	0.53	0.09	3	1.96	No column
B9	Sd	0.27	0.03	0.52	0.05	3	1.96	No column
B6	Gn	0.25	0.03	0.48	0.04	3	1.94	With column
B12	Gn	0.19	0.03	0.37	0.06	3	1.96	With column
B13	Gn	0.21	0.03	0.43	0.01	3	1.99	With column
B14	Gn	0.28	0.03	0.54	0.01	3	1.96	With column
2012878-26	Pyroclastics	0.37	0.02	0.73	0.00	3	1.99	With column
-32	Quartz diorite	0.37	0.05	0.72	0.01	3	1.98	With column
-34	Porphyritic monzogranite	0.49	0.03	1.05	0.04	3	2.13	With column
-36	Dolerite	0.36	0.05	0.70	0.07	3	1.96	With column
	Repeated	0.36	0.04	0.67	0.07	3	1.86	With column
-64	Rhyolite porphyry	0.33	0.02	0.69	0.04	3	2.09	With column

N represents the times of repeat measurements of the same purification solution in a single analytical session by MC-ICP-MS.
2SD = 2 times the standard deviation of the population of n repeat measurements of a sample solution.
Repeat: repeat sample dissolution, column chemistry and instrument analysis.
Mineral abbreviation: sphalerite (Sp); galena (Gn); siderite (Sd).

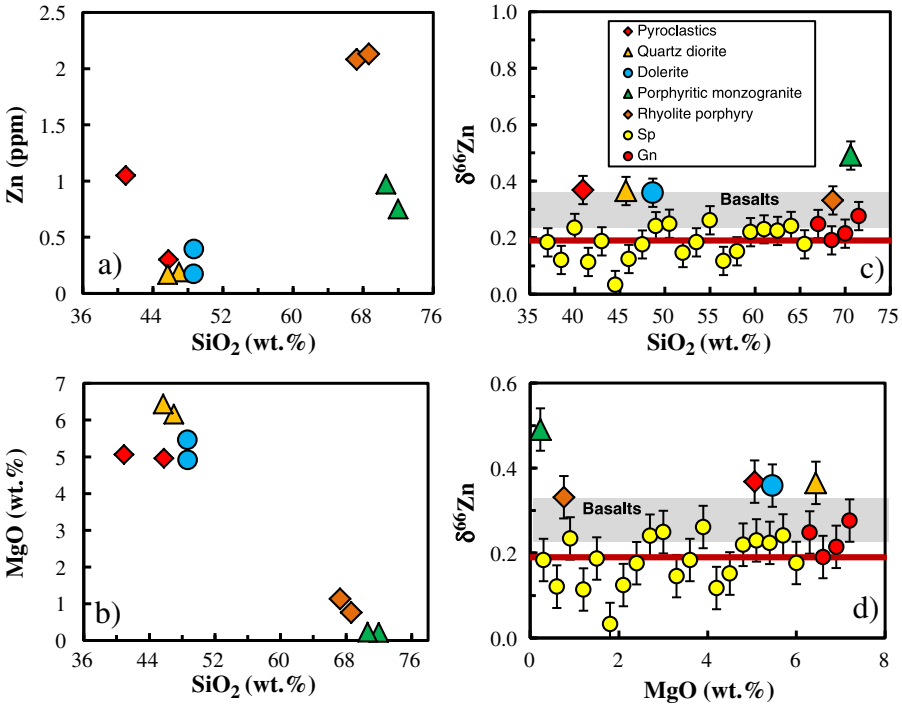

Fig. 4. Variation of Zn concentrations (a) and MgO contents (b) as a function of SiO_2 for igneous rocks from the Zhaxikang. Zinc isotopic variations ($\delta^{66}Zn$ relative to JMC-Lyon) of igneous rocks from the Zhaxikang Pb—Zn deposit as a function of SiO_2 (c) and MgO (d). For comparison, sulfide separates (sphalerite and galena) from the Zhaxikang are also plotted. Data of major elements and Zn concentration are from Lin (2014) and Zn isotope data are from Table 1 in this study. The field of MORB Zn isotopic composition is from Chen et al. (2013).

Table 3
In-situ Pb isotope data of sulfide separates from the Zhaxikang Pb—Zn deposit, South Tibet.

Sample spots	$^{206}Pb/^{204}Pb$	1SE	$^{207}Pb/^{204}Pb$	1SE	$^{208}Pb/^{204}Pb$	1SE
ZK1502-378.2-GN-1	19.704	0.001	15.877	0.001	40.419	0.004
ZK1502-378.2-GN-2	19.716	0.001	15.900	0.001	40.537	0.003
ZK1502-378.2-GN-3	19.686	0.001	15.857	0.001	40.339	0.005
ZK1502-378.2-GN-4	19.687	0.001	15.867	0.001	40.383	0.003
ZK1502-378.2-GN-5	19.687	0.001	15.861	0.001	40.361	0.003
ZK1502-378.2-SPH-1	19.362	0.026	15.702	0.019	39.826	0.051
ZK1502-378.2-SPH-2	19.073	0.062	15.571	0.050	39.287	0.128
ZK1502-378.2-SPH-3	19.095	0.026	15.588	0.021	39.369	0.054
ZK1502-378.2-SPH-4	19.000	0.029	15.516	0.021	39.205	0.057
ZK1502-378.2-SPH-5	18.727	0.036	15.355	0.029	38.685	0.073
ZK007-730-GN-1	19.890	0.002	15.848	0.002	40.351	0.004
ZK007-730-GN-2	19.896	0.002	15.855	0.001	40.374	0.004
ZK007-730-GN-3	19.894	0.002	15.855	0.001	40.378	0.004
ZK007-730-GN-4	19.895	0.001	15.855	0.001	40.372	0.003
ZK007-730-GN-5	19.895	0.001	15.853	0.001	40.368	0.003
ZK007-730-GN-6	19.887	0.002	15.851	0.002	40.357	0.005
ZK007-730-SPH-1	19.458	0.044	15.735	0.032	39.778	0.085
ZK007-730-SPH-2	18.941	0.093	15.582	0.075	39.038	0.189
ZK007-730-SPH-3	19.055	0.068	15.648	0.052	39.193	0.136
ZK007-730-SPH-4	19.209	0.038	15.663	0.028	39.438	0.076
ZK007-730-SPH-5	19.376	0.036	15.700	0.027	39.654	0.071

5.2. Sources of sulfur, lead and zinc in the Zhaxikang Pb—Zn deposit

Both Pb and S isotopic compositions of sulfides (sphalerite and galena) from the Zhaxikang Pb—Zn deposit display a wide range (Figs. 5 and 6). Most samples have highly radiogenic Pb isotopic compositions (e.g., $^{206}Pb/^{204}Pb = 18.727–19.896$), evolving towards upper crustal sediments. They are also more radiogenic than the regional igneous rocks ($^{206}Pb/^{204}Pb = 18.4–19.2$; Zhao et al., 2007), indicating a significant contribution from sedimentary rocks. As shown in Fig. 6, sulfur isotopic ratios of these sulfides (6‰–12‰; Fig. 6) are significantly higher than the mantle value (0 ± 2‰) and lighter than the values of sedimentary black shales in the region (10.94–11.49‰, average = 11.21‰; Li, 2010). These data indicate that Pb and S in these sulfides were derived from a mixing of regional sedimentary (e.g., shales) and igneous rocks. A simple calculation suggests that a large proportion of Pb in galena seems to be derived from regional lithologies (e.g., shales), with a relatively smaller proportion of Pb in sphelerites derived from shales. Sulfur isotopic compositions of sphalerites and galena also show a mixing of regional sedimentary and igneous rocks (Fig. 6).

It is noted that different types of sulfides from the Zhaxikang Pb—Zn deposit have different Pb and S isotopic compositions (Figs. 5 and 6). Sphalerite (ZnS) generally has higher S isotopic compositions but less radiogenic Pb isotopic composition than galena (PbS). For both sphalerite and galena, Zn isotopic compositions are not significantly different (Table 2), indicating that inter-mineral Zn isotope fractionation between sphalerite and galena is possibly negligible. This accounts for the similar Zn isotopic compositions but significant differences of S and Pb isotopic compositions between sphalerite and galena, although the contributions from sedimentary rocks and the basement rocks are different for those two minerals. Pb contents are high in crustal rocks and thus probably provided most of Pb for the galena. This hypothesis may explain the spatial zoning of major ore-forming minerals in the Zhaxikang deposit and is needed to be clarified by future studies.

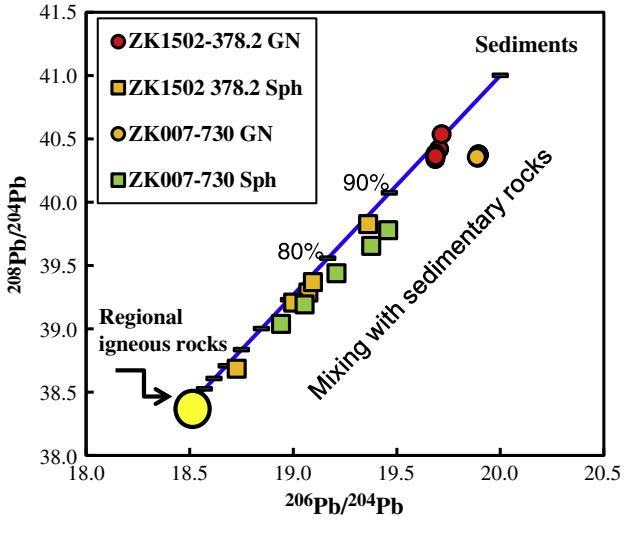

Fig. 5. Pb isotope evolution of sulfides (sphalerite and galena) from the Zhaxikang Pb—Zn deposit. The Pb isotope data are reported in Table 2. The data for regional igneous rocks and sedimentary rocks are from Lin (2014). The results show that Pb isotopic compositions of these sulfides are from mixing of basement rocks and sedimentary rocks at various proportions.

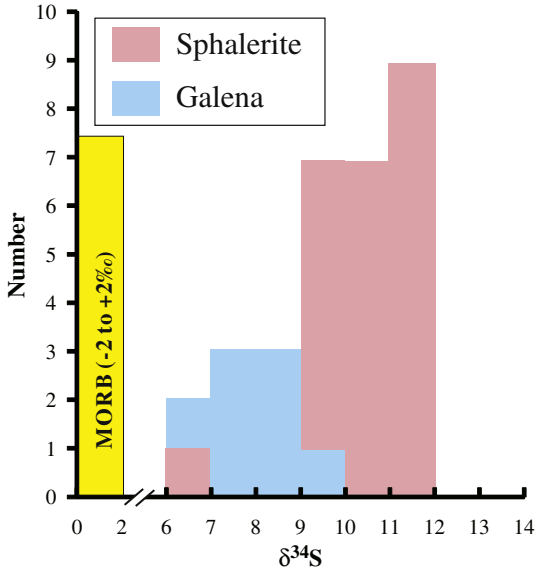

Fig. 6. Histogram of sulfur isotopic ratios ($\delta^{32}S$) of sulfides (sphalerite and galena) from the Zhaxikang Pb—Zn deposit. The data are from previous studies (Yang et al., 2006; Yang et al., 2009; Zhang et al., 2010; Li, 2010). The field of MORB sulfur isotopic composition is from Chaussidon and Lorand (1990).

Both S and Pb isotopes show a mixing of regional sedimentary rocks and igneous rocks, which may be used to constrain the origin of Zn. Before evaluating the potential of using Zn isotopes to trace the source of ore-forming metals, possible Zn isotope fractionation and magnitude of the fractionation should be taken into account. Several processes may be considered to potentially cause Zn isotope variation during ore-forming activity (Zhou et al., 2014a, 2014b), including: (1) temperature effects (Mason et al., 2005; Toutain et al., 2008), (2) mixing of multiple zinc sources (Wilkinson et al., 2005; Zhou et al., 2014a), and/or (3) kinetic Raleigh fractionation during mineral precipitation (Kelley et al., 2009; Gagnevin et al., 2012).

In theory, equilibrium isotope fractionation is a function of temperature, with larger fractionation generated at lower temperatures (Urey, 1947). However, the experimental studies by Maréchal and Sheppard (2002) demonstrate that there is limited Zn isotope variation in a temperature range from 30 to 50 °C. Based on a systematic study of sphalerites formed over a range of well-constrained precipitation conditions, Wilkinson et al. (2005) also suggested that there is no obvious correlation between Zn isotopic ratios and temperatures ranging widely from 60 to 250 °C, for Pb—Zn deposits of the Irish Midlands. These results indicate that the temperature effect on Zn isotope fractionation during hydrothermal processes is probably weak. The fluid inclusions in carbonates and sphalerite from the Zhaxikang Pb—Zn deposit have a median homogenization temperature of ~250 °C, and the late-stage Sb—Pb hydrothermal mineralization has a slightly lower homogenization temperature of ~230 °C (Lin, 2014). Therefore, although the homogenization temperature gradually decreases from early to late stages of mineralization in the Zhaxikang deposit, the temperature variation is not expected to significantly modify Zn isotopic compositions of sulfides formed in a hydrothermal system.

Rayleigh distillation can fractionate Zn isotopes in hydrothermal fluids, with increasing δ^{66}Zn values from early to late stages due to the precipitation of ^{64}Zn-enriched sulfides (e.g., sphalerite). This is similar to the case of Cu isotope variation generated at different stages of mineralization in porphyry and hydrothermal systems (Mathur et al., 2009). The Rayleigh mechanism has been used to explain the large Zn isotope variations observed in several deposits of various types such as VHMS (Mason et al., 2005), Irish-type (Wilkinson et al., 2005; Gagnevin et al., 2012) and SEDEX (Kelley et al., 2009). For example, it is likely that the incoming metal-bearing fluids varied by >0.2‰ in δ^{66}Zn values (Gagnevin et al., 2012). Theoretical calculations show that Zn isotope fractionation between an aqueous Zn solution (e.g., $ZnCl(H_2O)_5$ or $ZnHCO_3(H_2O)_4$) and sulfide species (e.g., $ZnS(HS)H_2O$, $Zn(HS)_4^{2-}$) is 0.2‰ at ~300 °C (Fujii et al., 2011). The sphalerites and galenas from the Zhaxikang Pb—Zn deposit were formed at the early stage of mineralization, and these samples were collected from a large area of >1 km^2 (Fig. 2). However, all samples display a small variation of δ^{66}Zn values from 0.03 to 0.28‰ with an average of 0.19 ± 0.10‰ (n = 25; 2SD). This may indicate a very limited rate of input of hydrothermal fluids during sphalerite precipitation, and/or much slower sphalerite growth rates, allowing isotopic re-equilibration within the fluids from which sphalerites were deposited to be obtained. Alternatively, it is possible that the amount of Zn in the precipitated sphalerites was not large enough to change the Zn reservoir of the hydrothermal fluids and this explains why the sphalerites show relatively homogeneous Zn isotope composition. When the Zn isotope fractionation between hydrothermal solutions and sulfides (0.2‰) is considered (Fujii et al., 2011), the δ^{66}Zn values of the hydrothermal fluids are calculated to be 0.39 ± 0.10‰ (2SD).

The Fe—Mn carbonates which occur as veins that cut the orebody have a homogeneous δ^{66}Zn value of 0.27 ± 0.06‰. Fluid inclusions in the Fe—Mn carbonates are Zn-enriched (Lin, 2014), pointing to a close relationship with Zn sulfides (Zhu et al., 2012). These carbonates, which occur as gangue minerals, were precipitated by hydrothermal fluids that infilled fractures (Fig. 3g, h and i; Lin, 2014), and thus their δ^{66}Zn values were taken to represent Zn isotopic composition of the hydrothermal fluids. These values are consistent within error with that calculated from Zn isotope fractionation between hydrothermal solutions and sulfides as discussed above. Zinc isotopic compositions of the hydrothermal solutions are similar to those of the regional unaltered igneous rocks spatially associated with the deposit (e.g., porphyritic monzogranite, dolerite etc. Fig. 2), providing strong evidence that igneous rocks were the main source of Zn in the sulfides.

However, the range of Zn isotopic composition in the sulfides (~0.3‰) is larger than that in the igneous rocks (~0.16‰) in Zhaxikang. This implies that at least Zn in these sulfides was partly derived from other sources. Compared with igneous rocks, sedimentary rocks commonly display larger Zn isotope range of up to 0.8‰ Maréchal et al. (2000); Weiss et al., 2007; Bentahila et al., 2008; Lv et al., 2016; Little et al., 2016). Consistent with the information provided by S and Pb isotopes, the Zn isotope data also suggest that sedimentary rocks (e.g., shales) are a significant source of metals in the Zhaxikang Pb—Zn deposits. However, the Zn isotopic compositions of sphalerite and galena samples studied here are substantially different from those of marine carbonates (with δ^{66}Zn up to 1.32‰; Pichat et al., 2003). We conclude that marine carbonate-derived Zn in the Zhaxikang Pb—Zn deposit is limited, or the potential contribution of Zn from carbonates is so low that it cannot be expressed in the Zn isotope system. The similar Zn isotopic compositions of sphalerite and galena with the hydrothermal carbonates further support the magmatic-hydrothermal origin of the Zn-sulfides.

5.3. Constraints on the ore genesis of the Zhaxikang Pb—Zn deposit

The Zn isotopic differences among different types of Pb—Zn deposits may be useful for suggesting a model of ore genesis. Sphalerite separates from MVT deposits in different regions have δ^{66}Zn values of −0.06 to +0.42‰ (Albarède, 2004), −0.32 to +0.23‰ (Gagnevin et al., 2012) whereas Irish-type deposits have a range of −0.17 to +1.33‰ (Wilkinson et al., 2005). Sphalerite separates from the Alexandrinka VHMS deposit in Russia have δ^{66}Zn values of −0.43 to +0.23‰ (Mason et al., 2005) and those from the Red Dog SEDEX deposit in the USA have δ^{66}Zn value of 0.00 to +0.60‰ (Kelley et al.,

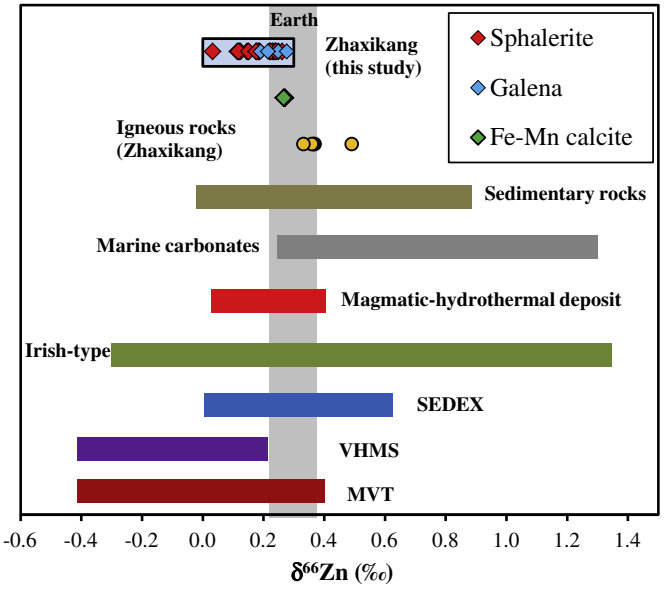

Fig. 7. Comparison of zinc isotopic compositions (δ^{66}Zn relative to JMC-Lyon) of sulfide separates from the Zhaxikang Pb—Zn deposit with data from various types of Pb—Zn deposits worldwide. Data sources: sedimentary rocks (Maréchal et al., 2000; Weiss et al., 2007; Bentahila et al., 2008; Lv et al., 2016; Little et al., 2016), the Earth (Chen et al., 2013), and marine carbonate (Pichat et al., 2003), Irish-type (Wilkinson et al., 2005; Gagnevin et al., 2012), SEDEX (Kelley et al., 2009), magmatic type (Maréchal et al., 1999), VHMS (Mason et al., 2005), MVT (Albarède, 2004).

2009) (Fig. 7). The overlap of Zn isotopic composition among deposits with different origins suggests that Zn isotopes may not be suitable for discriminating ore genesis of all types of deposits (Zhou et al., 2014a, 2014b). However, some important differences clearly exist (Fig. 7): (i) magmatic-hydrothermal deposits have a narrow δ^{66}Zn range, (ii) VHMS and MVT mineral systems generally have relatively light δ^{66}Zn values, and (iii) SEDEX systems have heavy δ^{66}Zn values which are absent in other types of Pb—Zn deposits. The causes for these differences are not well understood, but are likely related to source rocks, temperature, and duration of hydrothermal processes.

The Zhaxikang Pb—Zn deposit in South Tibet is one of the largest Pb—Zn deposits in China (1.2 Mt, Pb + Zn + Sb), but its genesis remains highly debated. Models that have been proposed include SEDEX-type related to reworking by hydrothermal fluids based on studies of H—O isotopes (Zheng et al., 2012), low sulphidation epithermal hot spring (Meng et al., 2008), or magmatic-hydrothermal (Lin, 2014; Zhu et al., 2012; Li, 2010). Evidence for a SEDEX origin includes the colloform textures of the ores, and the presence of large amounts of sedimentary carbonate rocks forming the wall rocks. Our results show that Zn isotopic compositions of sphalerites and galenas from the Zhaxikang Pb—Zn deposit are significantly different from those of typical SEDEX Pb—Zn deposits (Fig. 7). In addition, Zn isotopes show no evidence for the involvement of marine carbonates, which have very heavy δ^{66}Zn relative to igneous rocks (up to ~1.3‰; Pichat et al., 2003). The proposed model, based on H, O and Si isotopes, suggests that epithermal hot springs were probably an important source of fluids (Meng et al., 2008). However, the hydrothermal solutions generally have heavy δ^{66}Zn values relative to igneous rocks (Chen et al., 2014b), and thus they should not have provided significant amounts of Zn even if hydrothermal solutions may constitute an important contribution. To date, there is no exhaustive database of δ^{66}Zn data for SEDEX, VHMS, and MVT mineral systems. More work is future required to fill this gap. As shown in this study, Zn may have been mainly sourced from crust-derived felsic igneous rocks with contribution from sedimentary rocks, and the genesis of the Zhaxikang Pb—Zn deposit was most likely related to mid-low temperature magma-related hydrothermal activity. Zircon U—Pb and Ar—Ar isotope ages (~20 Ma) show that some of the igneous rocks in the Zhaxikang region were formed almost synchronously with the deposit (Lin, 2014), supporting the magmatic-hydrothermal origin for the Zhaxikang Pb—Zn deposit.

6. Conclusions

Zinc and lead isotopic ratios of sulfides (sphalerite and galena), Fe—Mn carbonates and associated basement rocks from the Zhaxikang Pb—Zn deposit, Tibet, were studied to provide possible constraints on the origin of this deposit. Both S and Pb isotopes of sphalerite and galena from the Zhaxikang Pb—Zn deposit show large variations, falling between the values of basement rocks and sedimentary rocks (e.g., shales). In particular, different types of minerals display different S and Pb isotopic compositions. These results indicate that S and Pb in the Zhaxikang deposit were derived from a mixing of igneous rocks and sedimentary rocks in various proportions.

The main sulfides (sphalerite and galena) from Zhaxikang show a small range of δ^{66}Zn from +0.03 to +0.28‰ with an average of +0.19 ± 0.10‰. When the Zn isotope fractionation between hydrothermal solution and sulfides (0.2‰) is considered (Fujii et al., 2011), the δ^{66}Zn values of the hydrothermal fluids are calculated to be 0.39 ± 0.10‰ (2SD). This value is consistent within error with that of regional igneous rocks (0.36 ± 0.03‰) spatially and temporally associated with the deposit, and therefore suggests that Zn was mainly derived from igneous rocks. The Fe—Mn carbonates, which occur as veins, were formed by hydrothermal processes related to magmatic activity. Their δ^{66}Zn values (+0.27‰ ± 0.05‰) are taken to represent Zn isotopic composition of the hydrothermal fluids. The δ^{66}Zn values of sphalerite and galena are also consistent, within error, to those of the Fe—Mn carbonates. Notably, however, the range of Zn isotopic composition in these sulfides is larger than that of most igneous rocks in Zhaxikang, implying that at least Zn in these sulfides was partly derived from sedimentary rocks which commonly display large Zn isotope range of up to ca. 1.0‰. Consistent with the results from S and Pb isotopes, the Zn isotope data also suggest that sedimentary rocks (e.g., shales) are a significant source of metals including Zn in the Zhaxikang Pb—Zn deposits. In conclusion, our results from Zn and Pb isotopes suggest a possible magmatic-hydrothermal origin for the Zhaxikang Pb—Zn deposit.

Acknowledgement

We thank Drs. Linkui Zhang, Lukas Zurcher, David Lentz and Sheng-Ao Liu for discussion. Dr. Wenbao Zheng and Dr. Pan Tang are thanked for the help in the field and office. We also thank Dr. Leon Bagas and Sean H. McClenaghan for their careful revisions and anonymous reviewers' encouragement, which significantly improved the manuscript. This work is supported by Special Industry Fund (201511022-02) and Geological Survey Project (12120114050701).

References

Albarède, F., 2004. The stable isotope geochemistry of copper and zinc. Rev. Mineral. Geochem. 55, 409–427.
Archer, C., Vance, D., 2004. Mass discrimination correction in multiple-collector plasma source mass spectrometry: an example using Cu and Zn isotopes[J]. J. Anal. At. Spectrom. 19 (5), 656–665.
Bentahila, Y., Othman, D.B., Luck, J.M., 2008. Strontium, lead and zinc isotopes in marine cores as tracers of sedimentary provenance: a case study around Taiwan orogen. Chem. Geol. 248, 62–82.
Borrok, D.M., Wanty, R.B., Ridley, W.I., Wolf, R., Lamothe, P.J., Adams, M., 2007. Separation of copper, iron, and zinc from complex aqueous solutions for isotopic measurement. Chem. Geol. 242, 400–414.
Chaussidon, M., Lorand, J.P., 1990. Sulphur isotope composition of orogenic spinel lherzolite massifs from Ariege (North-Eastern Pyrenees, France): an ion microprobe study[J]. Geochim. Cosmochim. Acta 54 (10), 2835–2846.
Chen, H., Savage, P.S., Teng, F.Z., Helz, R.T., Moynier, F., 2013. Zinc isotope fractionation during magmatic differentiation and the isotopic composition of the bulk Earth. Earth Planet. Sci. Lett. 369, 34–42.
Chen, K., Yuan, H., Bao, Z., Zong, C., Dai, M., 2014a. precise and accurate in situ determination of lead isotope ratios in NIST, USGS, MPI-DING and CGSG glass reference materials using femtosecond laser ablation MC-ICP-MS. Geostand. Geoanal. Res. 38, 5–21.
Chen, J.B., Gaillardet, J., Dessert, C., Villemant, B., Louvat, P., Crispi, O., Birck, J.L., Wang, Y.N., 2014b. Zn isotope compositions of the thermal spring waters of La Soufrière volcano, Guadeloupe Island. Geochim. Cosmochim. Acta 127, 67–82.
Dauphas, N., Pourmand, A., Teng, F.-Z., 2009. Routine isotopic analysis of iron by HR-MC-ICPMS: how precise and how accurate? Chem. Geol. 267, 175–184.
Dekov, V.M., Cuadros, J., Kamenov, G.D., 2010. Metalliferous sediments from the HMS Challenger voyage (1872-1876). Geochim. Cosmochim. Acta 74, 5019–5038.
Fujii, T., Moynier, F., Pons, M.L., 2011. The origin of Zn isotope fractionation in sulfides[J]. Geochim. Cosmochim. Acta 75 (23), 7632–7643.
Gagnevin, D., Boyce, A., Barrie, C., Menuge, J., Blakeman, R., 2012. Zn, Fe and S isotope fractionation in a large hydrothermal system. Geochim. Cosmochim. Acta 88, 183–198.
John, S.G., Conway, T.M., 2014. A role for scavenging in the marine biogeochemical cycling of zinc and zinc isotopes[J]. Earth Planet. Sci. Lett. 394, 159–167.
John, S., Rouxel, O., Craddock, P., Engwall, A., Boyle, E., 2008. Zinc stable isotopes in seafloor hydrothermal vent fluids and chimneys. Earth Planet. Sci. Lett. 269, 17–28.
Kapp, P., DeCelles, P., Leier, A., Fabijanic, J., He, S., Pullen, A., Gehrels, G., Ding, L., 2007. The Gangdese retroarc thrust belt revealed. GSA Today. 17, p. 4.
Kelley, K., Wilkinson, J., Chapman, J., Crowther, H., Weiss, D., 2009. Zinc isotopes in sphalerite from base metal deposits in the Red Dog district, Northern Alaska. Econ. Geol. 104, 767–773.
Kunzmann, M., Halverson, G.P., Sossi, P.A., et al., 2013. Zn isotope evidence for immediate resumption of primary productivity after snowball Earth[J]. Geology 41 (1), 27–30.
Li, G., 2010. Element and Isotope Geochemistry of the Zhaxikang Sb-Pb-Zn Polymetallic Deposit. Tibet, Master Dissertation.
Liang, W., Hou, Z., Yang, Z., Li, Z., Huang, K., Zhang, S., Li, W., Zheng, Y., 2013. Remobilization and overprinting in the Zhaxikang Pb-Zn-Ag-Sb polymetal ore deposit, Southern Tibet: implications for its metallogenesis. Acta Geol. Sin. 29, 3828–3842.
Lin, B., 2014. Geologic Features and Genesis Discussion of Zhaxikang Zinc Polymetallic Deposit in Tibet Master Dissertation.
Lin, B., Tang, J., Zheng, W., Leng, Q., Wang, Y., Liu, M., Yang, H., Ding, S., Zhang, L., Yang, H., 2013. Geological characteristics and modes of occurrence of silver in Zhaxikang zinc polymetallic deposit. Mineral Deposits 32, 899–914.
Little, S.H., Vance, D., Walker-Brown, C., Landing, W.M., 2014. The oceanic mass balance of copper and zinc isotopes, investigated by analysis of their inputs, and outputs to ferromanganese oxide sediments. Geochim. Cosmochim. Acta 125 (2014), 673–693.

Little, S.H., Vance, D., McManus, J., et al., 2016. Key role of continental margin sediments in the oceanic mass balance of Zn and Zn isotopes[J]. Geology 44 (3), 207–210.
Liu, S.A., Li, D.D., Li, S.-G., Teng, F.-Z., Ke, S., He, Y.-S., Lu, Y.-H., 2014. High-precision copper and iron isotope analysis of igneous rock standards by MC-ICP-MS. J. Anal. At. Spectrom. 29, 122–133.
Lv, Y.W., Liu, S.A., Zhu, J.M., Li, S.G., 2016. Copper and zinc isotope fractionation during deposition and weathering of highly metalliferous black shales in Central China. Chem. Geol. 422, 82–93.
Maréchal, C.N., Sheppard, S.M.F., 2002. Isotopic fractionation of Cu and Zn between chloride and nitrate solutions and malachite or smithsonite at 30 °C and 50 °C Goldschmidt Conference Geochim. Cosmochim. Acta 66, A484.
Maréchal, C.N., Télouk, P., Albarède, F., 1999. Precise analysis of copper and zinc isotopic compositions by plasma-source mass spectrometry. Chem. Geol. 156, 251–273.
Maréchal, C.N., Emmanuel, N., Chantal, D., Francis, A., 2000. Abundance of zinc isotopes as a marine biogeochemical tracer. Geochem. Geophys. Geosyst. 1, 1999GC–000029.
Mason, T.F., Weiss, D.J., Chapman, J.B., Wilkinson, J.J., Tessalina, S.G., Spiro, B., Horstwood, M.S., Spratt, J., Coles, B.J., 2005. Zn and Cu isotopic variability in the Alexandrinka volcanic-hosted massive sulfide (VHMS) ore deposit, Urals, Russia. Chem. Geol. 221, 170–187.
Mathur, R., Titley, S., Barra, F., Brantley, S., Wilson, M., Phillips, A., Munizaga, F., Maksaev, V., Vervoort, J., Hart, G., 2009. Exploration potential of Cu isotope fractionation in porphyry copper deposits. J. Geochem. Explor. 102, 1–6.
Meng, X.J., Yang, Z.S., Qi, X.X., 2008. Silicon-oxygen-hydrogen isotopic compositions of Zaxikang antimony polymetallic deposit in southern Tibet and its responses to the ore-controlling structure. Acta Petrol. Sin. 24 (7), 1649–1655.
Nie, F.J., Hu, P., Jiang, S.H., Li, Z.Q., Liu, Y., Zhou, Y., 2005. Type and temporal-spatial distribution of gold and antimony deposits (prospects) in southern Tibet, China. Acta Geol. Sin. 79, 373–385.
Pichat, S., Douchet, C., Albarède, F., 2003. Zinc isotope variations in deep-sea carbonates from the eastern equatorial Pacific over the last 175 ka. Earth Planet. Sci. Lett. 210, 167–178.
Rosman, K.J.R., 1972. A survey of the isotopic and elemental abundances of zinc. Geochim. Cosmochim. Acta 36, 801–819.
Schoenberg, R., von Blanckenburg, F., 2005. An assessment of the accuracy of stable Fe isotope ratio measurements on samples with organic and inorganic matrices by high-resolution multicollector ICP-MS. Int. J. Mass Spectrom. 242, 257–272.
Sivry, Y., Riotte, J., Sonke, J., Audry, S., Schäfer, J., Viers, J., Blanc, G., Freydier, R., Dupré, B., 2008. Zn isotopes as tracers of anthropogenic pollution from Zn-ore smelters the Riou Mort–Lot river system. Chem. Geol. 255, 295–304.
Sossi, P.A., Halverson, G.P., Nebel, O., 2015. Combined separation of Cu, Fe and Zn from rock matrices and improved analytical protocols for stable isotope determination[J]. Geostand. Geoanal. Res. 39 (2), 129–149.
Telus, M., Dauphas, N., Moynier, F., Tissot, F.L., Teng, F.Z., Nabelek, P.I., Groat, L.A., 2012. Iron, zinc, magnesium and uranium isotopic fractionation during continental crust differentiation: The tale from migmatites, granitoids, and pegmatites. Geochim. Cosmochim. Acta 97, 247–265.
Toutain, J.P., Sonke, J., Munoz, M., Nonell, A., Polvé, M., Viers, J., Freydier, R., Sortino, F., Joron, J.L., Sumarti, S., 2008. Evidence for Zn isotopic fractionation at Merapi volcano. Chem. Geol. 253, 74–82.
Urey, H.C., 1947. The thermodynamic properties of isotopic substances. J. Chem. Soc. 562–581.
Wang, Y., Tang, J., Zheng, W., Bin, L., 2012. A tentative discussion on ore-fabric and genesis of the Zhaxikang Zn-polymetallic deposit, Lhunze County, Tibet. Acta Geol. Sin. 33, 681–692.
Weiss, D.J., Rausch, N., Mason, T.F.D., Coles, B.J., Wilkinson, J.J., Ukonmaanaho, L., et al., 2007. Atmospheric deposition and isotope biogeochemistry of zinc in ombrotrophic peat. Geochim. Cosmochim. Acta 71, 3498–3517.
Wilkinson, J., Weiss, D., Mason, T., Coles, B., 2005. Zinc isotope variation in hydrothermal systems: preliminary evidence from the Irish Midlands ore field. Econ. Geol. 100, 583–590.
Yang, Z., Hou, Z., Gao, W., Wang, H., Li, Z., 2006. Metallogenic charactristics and genetic model of antimony and gold deposits in South Tibetan detachment system. Acta Geol. Sin. 40, 671–680.
Yang, Z., Hou, Z., Meng, X., Liu, Y., Fei, H., Tian, S., Li, Z., Gao, W., 2009. Post-collisional Sb and Au mineralization related to the South Tibetan detachment system, Himalayan orogen. Ore Geol. Rev. 36, 194–212.
Yin, A., 2001. Geologic evolution of the Himalayan-Tibetan orogen in the context of phanerozoic continental growth of the Asia. Acta Geosci. Sin. 22 (3), 193–230 (in Chinese with english abstract).
Yin, A., Harrison, T.M., Murphy, M., Grove, M., Nie, S., Ryerson, F., Feng, W.X., Le, C.Z., 1999. Tertiary deformation history of southeastern and southwestern Tibet during the Indo-Asian collision. Geol. Soc. Am. Bull. 111, 1644–1664.
Zhang, G.Y., 2012. Zangnan Gold Antimony Polymetallic Metallogenic Belt of Metallogenic Model and Prospecting Prospect Ph.D Dissertation.
Zhang, J.F., Zheng, Y.Y., Zhang, G.-Y., Gao, S., Ye, X., Zhang, Z., Liu, M., Ji, Q., 2010. Genesis of Zhaxikang Pb—Zn—Sb—Ag deposit in Northern Himalaya: constraints from multi-isotope geochemistry. Earth science. J. China Univ. Geosci. 35, 1000–1010.
Zhao, Z., Mo, X., Dong, G., Zhou, S., Zhu, D., Liao, Z., Sun, C., 2007. Pb isotopic geochemistry of Tibetan plateau and it implications. Geoscience 21, 265–274.
Zhao, Y., Vance, D., Abouchami, W., et al., 2014. Biogeochemical cycling of zinc and its isotopes in the Southern Ocean[J]. Geochim. Cosmochim. Acta 125, 653–672.
Zheng, Y.Y., Liu, M.Y., Sun, X., Yuan, E.H., Tian, L.M., Zheng, H.T., Zhang, G.Y., Zhang, L.H., 2012. Type, discovery process and significance of Zhaxikang antimony ploymetallic ore deposit, Tibet. J. China Univ. Geosci. 37, 1003–1012.
Zheng, Y.Y., Sun, X., Liu, M.Y., Yuan, E.H., Tian, L.M., Zheng, H.T., Zhang, G.Y., Zhang, L.H., 2014. Mineralization, deposit type and metallogenic age of the gold antimony polymetallic belt in the eastern part of North Himalayan. Geotecton. Metallog. 38, 108–118.
Zhou, J.X., Huang, Z.L., Zhou, M.F., Zhu, X.K., Muchez, P., 2014a. Zinc, sulfur and lead isotopic variations in carbonate-hosted Pb—Zn sulfide deposits, southwest China. Ore Geol. Rev. 58, 41–54.
Zhou, J.X., Huang, Z.L., Lv, Z.C., Zhu, X.K., Gao, J.G., 2014b. Geology, isotope geochemistry and ore genesis of the Shanshulin carbonate-hosted Pb—Zn deposit, southwest China. Ore Geol. Rev. 63, 209–225.
Zhu, X.K., Guo, Y., Williams, R.J.P., O'Nions, R.K., Matthews, A., Belshaw, N.S., Canters, G.W., de Waal, E.C., Weser, U., Burgess, B.K., Salvato, B., 2002. Mass fractionation processes of transition metal isotopes. Earth Planet. Sci. Lett. 200, 47–62.
Zhu, L.K., Gu, X.X., Li, G.Q., Zhang, Y.M., Cheng, W.B., 2012. Fluid inclusions in the Zhaxikang Pb—Zn—Sb polymetallic deposit, South Tibet and its geological significance. Geoscience 26 (3), 453–463.